PAPER

Electron kinetics in a positive column of AC discharges in a dynamic regime

To cite this article: Nathan A Humphrey and Vladimir I Kolobov 2023 *Plasma Sources Sci. Technol.* **32** 085017

View the article online for updates and enhancements.

You may also like

- Monte Carlo-based estimation of uncertainty owing to limited resolution of digital instruments
- R B Frenkel and L Kirkup
- Inductively coupled plasmas at low driving frequencies
 Vladimir I Kolobov and Valery A Godyak
- Spatiotemporal Patterns Formed on p-Type Silicon Electrodes during Electrochemical Dissolution Yuya Suzuki, Tomoko Urata, Kazuhiro Fukami et al.



Plasma Sources Sci. Technol. 32 (2023) 085017 (17pp)

https://doi.org/10.1088/1361-6595/acee1c

Electron kinetics in a positive column of AC discharges in a dynamic regime

Nathan A Humphrey¹ and Vladimir I Kolobov^{2,*}

- ¹ The University of Alabama, Tuscaloosa, AL 35487, United States of America
- ² The University of Alabama in Huntsville, Huntsville, AL 35899, United States of America

E-mail: vladimir.kolobov@uah.edu

Received 4 June 2023, revised 25 July 2023 Accepted for publication 8 August 2023 Published 29 August 2023



Abstract

We have performed hybrid kinetic-fluid simulations of a positive column in alternating current (AC) argon discharges over a range of driving frequencies f and gas pressure p for the conditions when the spatial nonlocality of the electron energy distribution function (EEDF) is substantial. Our simulations confirmed that the most efficient conditions of plasma maintenance are observed in the dynamic regime when time modulations of mean electron energy (temperature) are substantial. The minimal values of the root mean square electric field and the electron temperature have been observed at f/p values of about 3 kHz Torr⁻¹ in a tube of radius R = 1 cm. The ionization rate and plasma density reached maximal values under these conditions. The numerical solution of a kinetic equation allowed accounting for the kinetic effects associated with spatial and temporal nonlocality of the EEDF. Using the kinetic energy of electrons as an independent variable, we solved an anisotropic tensor diffusion equation in phase space. We clarified the role of different flux components during electron diffusion in phase space over surfaces of constant total energy. We have shown that the kinetic theory uncovers a more exciting and rich physics than the classical ambipolar diffusion (Schottky) model. Non-monotonic radial distributions of excitation rates, metastable densities, and plasma density have been observed in our simulations at pR > 6 Torr cm. The predicted off-axis plasma density peak in the dynamic regime has never been observed in experiments so far. We hope our results stimulate further experimental studies of the AC positive column. The kinetic analysis could help uncover new physics even for such a well-known plasma object as a positive column in noble gases.

Keywords: electron kinetics, positive column, AC discharges, noble gases

(Some figures may appear in colour only in the online journal)

1. Introduction

A positive column is a classical object of gas discharge physics with essential applications in lighting and gas lasers [1]. The low-temperature plasma of the positive column can be axially uniform or striated depending on the gas type and discharge conditions. The plasma can be maintained by direct current (DC) or alternating current (AC) power sources over various

driving frequencies and gas pressures. The plasma properties are controlled by the balance of electron impact ionization and the ambipolar diffusion to the wall or volume recombination. Two distinct time scales determine the dynamic properties of positive column plasma: the ambipolar diffusion time, τ_a and the electron energy relaxation time τ_u . Depending on the AC angular frequency ω , three operating regimes have been identified [2]. In the low-frequency regime, $\omega \tau_a < 1$, the axial electric field, E_z , maintaining the plasma remains nearly constant during most of the AC period, and the plasma density follows the current oscillations (quasi-DC case). In the

^{*} Author to whom any correspondence should be addressed.

high-frequency regime, $\omega \tau_u > 1$, plasma density remains constant, and the electric field follows the current oscillations with a phase shift that depends on the ratio ν/ω of the electron collision frequency ν to the driving frequency. The intermediate case $\tau_a^{-1} < \omega < \tau_u^{-1}$ corresponds to a 'dynamic regime,' which is a focus of the present paper.

The dynamic regime found practical application in light sources: a noticeable increase of light intensity was observed in this regime [2, 3]. Experimental studies of the positive column of AC discharges in helium revealed surprising offaxis peaks of metastable atom density [4], which were attributed to peculiarities of electron kinetics and ionization processes in pulsed plasma. The off-axis peaks of excitation rates were first observed in simulations of DC positive columns [5, 6] and later explained theoretically [7] by peculiarities of nonlocal electron kinetics in noble gases at elevated gas pressures. The dynamic regime of an inductively coupled plasma (ICP) has been studied in [8] using a fluid model for electrons.

The present paper aims to study electron kinetics and ionization processes in the dynamic regime under conditions where the spatial nonlocality of electron kinetics may be significant. Kinetic simulations of nonlocal electron kinetics in a steady-state DC positive column, where the energy and radial dependence of the electron energy distribution function (EEDF) cannot be factorized $f_0(u,r) \neq f_0^0(u) n_e(r)$, have been previously reported (see [9, 10] and references therein). Many publications have been devoted to solving the local Boltzmann equation for the EEDF and analysis of temporal nonlocality when the EEDF is a nonlocal function of time $f_0(u,t) \neq f_0^0(u) n_e(t)$ [1]. However, no analysis of spatially nonlocal electron kinetics under conditions of temporal nonlocality, where the EEDF is a complex function of all three arguments, has been performed so far. The present paper aims to address this deficiency for an AC positive column in a collision-dominated regime when the electron mean free path is smaller than the tube radius. We discuss the peculiarities of electron kinetics and ionization processes in this system and confirm that the optimal conditions for plasma maintenance occur in the dynamic regime.

2. Computational model

The hybrid model used in the present paper was first described in [11] and later adapted in [12] to study plasma stratification in noble gases. Here, this model is used to study the AC positive column in the collisional plasma of noble gases.

2.1. Kinetic equation for electrons

By using the two-term spherical harmonics expansion for the electron distribution function, $f_{\rm e} = f_0 + \frac{\nu}{\nu} \cdot f_1$, the Boltzmann kinetic equation for electrons in weakly ionized collisional plasma can be reduced to a set of coupled differential equations describing the isotropic component f_0 and anisotropic component f_1 (sometimes called Davydov–Allis system) [13–15]:

$$\frac{\partial f_0}{\partial t} + \frac{v}{3} \nabla \cdot f_1 - \frac{1}{3v^2} \frac{\partial}{\partial v} \left(v^2 \frac{eE}{m} \cdot f_1 \right) = S_0 \tag{1}$$

$$\frac{\partial \mathbf{f}_{1}}{\partial t} + v \nabla f_{0} - \frac{e\mathbf{E}}{m} \frac{\partial f_{0}}{\partial v} = -\nu (v) \mathbf{f}_{1}. \tag{2}$$

Here, ∇ denote the divergence and gradient operators in configuration (physical) space, e and m are the unsigned electron charge and electron mass, \mathbf{E} is the electric field vector, $\nu(v)$ is the transport collision frequency, and S_0 is the collision term describing energy loss in collisions and the production of new electrons.

Using the electron kinetic energy $u = mv^2/(2e)$ expressed in eV, equation (1) can be rewritten in the form

$$\frac{\partial f_0}{\partial t} + \nabla \cdot \mathbf{\Phi} - \frac{1}{\nu} \frac{\partial}{\partial u} (\nu \Gamma) = S_0, \tag{3}$$

where

$$\mathbf{\Phi} = \frac{v}{3} \mathbf{f}_1, \quad \Gamma = \mathbf{E} \cdot \mathbf{\Phi} \tag{4}$$

is the spatial flux, and Γ is the flux along energy in phase space. We consider conditions when the angular frequency of the electric field variation ω is low compared to $\nu(v)$. In this case, the spatial flux becomes

$$\Phi = -D_r \left(\nabla f_0 - E \frac{\partial f_0}{\partial u} \right) \tag{5}$$

where $D_r = v^2/(3\nu)$ is the spatial diffusion coefficient. Substituting (4) into (3), we obtain the kinetic equation for f_0 in the form of a diffusion equation in the 4-dimensional phase space (r, u):

$$\frac{\partial f_0}{\partial t} - \nabla_4 \cdot (\mathbf{D} \nabla_4 f_0) = S_0. \tag{6}$$

Here ∇_4 denotes the divergence and gradient operators in a 4-dimensional phase space (r,u). The speed v becomes the Lame coefficient, and **D** is the tensor:

$$\mathbf{D} = D_r \begin{pmatrix} I_3 & -\mathbf{E} \\ -\mathbf{E} & \mathbf{E}^2 \end{pmatrix} \tag{7}$$

where I_3 denotes the unit tensor in configuration space. The kinetic equation (6) has been used (in 2D phase space) for the analysis of the axial and radial structure of DC discharges and plasma stratification [16]. It has also appeared in the study of fully-ionized plasma [17].

The diagonal elements of the tensor (7) describe electron diffusion in the configuration space and electron diffusion along the kinetic energy axis with the diffusion coefficient, $D_u = D_r(E \cdot E)$, which corresponds to Joule heating. The heating does not depend on the direction of the electric field—it is determined by the absolute value of the electric field at a given point. The off-diagonal terms in the diffusion tensor describe additional fluxes in phase space associated with gradients in configuration and velocity space. We aim to clarify the nature of these fluxes under nonlocal electron kinetics conditions.

Specific source terms S_0 for quasi-elastic, inelastic, and Coulomb collisions can be found in [11, 17, 18]. The quasi-elastic collisions and Coulomb interactions contribute a differential (Fokker–Planck) term to the energy flux Γ (see below). Inelastic collisions and ionization processes result in significant energy jumps and change in the number of particles.

2.2. Hybrid model of positive column

Using cylindrical coordinates in configuration space is convenient to describe an axisymmetric positive column plasma inside a cylindrical tube. In an axially homogeneous plasma $(\partial/\partial z = 0)$, the electric field can be separated into axial and radial components. These components evolve at different time scales. The axial component, E_z , maintaining the plasma is controlled by the external current source. The radial component, E_r , is generated by the plasma to support quasi-neutrality. This component evolves at a time scale controlled by the variation in the EEDF f_0 and by ion transport.

The kinetic equation (6) for the positive column becomes [10]:

$$\begin{split} &\frac{\partial f_{0}}{\partial t} - \frac{1}{r} \frac{\partial}{\partial r} \left[r D_{r} \left(\frac{\partial f_{0}}{\partial r} - E_{r} \frac{\partial f_{0}}{\partial u} \right) \right] \\ &+ \frac{1}{v} \frac{\partial}{\partial u} \left[v E_{r} D_{r} \left(\frac{\partial f_{0}}{\partial r} - E_{r} \frac{\partial f_{0}}{\partial u} \right) \right] - \frac{1}{v} \frac{\partial}{\partial u} \left(v \Gamma_{u} \right) = S_{0}^{*} \quad (8) \end{split}$$

where the electron flux along the energy axis Γ_u is due to electron heating by the axial electric field $E_z(t)$ and energy loss in quasi-elastic collisions described by the Fokker–Planck form. The term S_0^* describes inelastic collisions. The electron fluxes in phase space (r,u) are:

$$\Phi_r = -D_r \left(\frac{\partial f_0}{\partial r} - E_r \frac{\partial f_0}{\partial u} \right) \tag{9}$$

$$\Gamma = -E_{\rm r}\Phi_r - D_u \frac{\partial f_0}{\partial u} - V_u f_0 = -E_{\rm r}\Phi_r - \Gamma_u \qquad (10)$$

where $D_u(t) = D_r E_z^2$ is a diffusion coefficient, $V_u = \delta \nu u$ is an advection velocity, and δ is a fraction of electron energy lost in quasi-elastic collisions of electrons with neutrals.

It is essential to point out that the radial (ambipolar) and the axial (conductive) electric fields play different roles in equation (8). The axial electric field $E_z(t)$ contributes to electron heating via the term $D_u \frac{\partial f_0}{\partial u}$. The radial field, $E_r = -\nabla \varphi$, describes electron diffusion in phase space (r,u) over surfaces of constant total energy $\varepsilon = u - \varphi(r,t)$, where $\varphi(r,t)$ is the electrostatic potential.

In the present work, the electric field $E_z(t)$ was calculated as [4]:

$$E_z(t) = \frac{I(t)}{2\pi \int_0^R \mu_e(r,t) n_e(r,t) r dr}$$
(11)

where μ_e is the electron mobility, and n_e is the electron density. The discharge current was prescribed in the form,

 $I(t) = I_0 \sin \omega t$. As shown below, at low frequencies, the time variation of the electric field $E_z(t)$ can be un-harmonic even for a mono-harmonic variation of the discharge current.

The radial electrostatic potential is calculated by solving the Poisson equation:

$$\frac{\epsilon_0}{r} \frac{\partial}{\partial r} r \frac{\partial \varphi}{\partial r} = n_{\rm i} - n_{\rm e} \tag{12}$$

where $n_{\rm e}$ and $n_{\rm i}$ are the electron and ion densities, and ϵ_0 is the permittivity of free space. The electron density is calculated from the EEDF f_0 as

$$n_{\rm e} = \int_0^\infty \sqrt{u} f_0 \mathrm{d}u. \tag{13}$$

Ions and metastable atoms are described using a driftdiffusion model:

$$\frac{\partial n_i}{\partial t} + \frac{1}{r} \frac{\partial}{\partial r} r \left(\mu_i n E_r - D_i \frac{\partial n_i}{\partial r} \right) = S_i \tag{14}$$

$$\frac{\partial n_m}{\partial t} + \frac{1}{r} \frac{\partial}{\partial r} r \left(-D_m \frac{\partial n_m}{\partial r} \right) = S_m \tag{15}$$

where μ_i and D_i are the ion mobility and diffusion coefficients of ions, $D_{\rm m}=D_{\rm i}$ is the diffusion coefficient of metastables, $S_{\rm i}$ is the ion production rate, and $S_{\rm m}$ is the metastable production rate according to the reactions shown in table 1. It is assumed that gas temperature and ion temperature are $T_{\rm i}=T_{\rm m}=T_{\rm g}=300~{\rm K}$.

The set of equations (8)–(15) satisfies scaling laws [19]: in a given gas, the positive column plasma in a tube radius R depends on pR, I/R, and f/p, where $f = \omega/2\pi$ is the cyclic frequency. Stepwise ionization and volume recombination via binary collisions do not violate the scaling laws, which break in the presence of three-body collisions and substantial deviations from quasi-neutrality.

The classical Schottky model for a positive column assumes (a) $S_i = n_e \nu_i (T_e)$, (b) $n_i = n_e = n$, (c) $\varphi(r) = T_e \ln(n_e)$, which results in the ambipolar diffusion equation for plasma density:

$$\frac{\partial n}{\partial t} - \frac{1}{r} \frac{\partial}{\partial r} r \left(D_{a} \frac{\partial n}{\partial r} \right) = n \nu_{i} \left(T_{e} \right) \tag{16}$$

where $D_a = \mu_i T_e$ is the ambipolar diffusion coefficient. This equation determines the value of T_e , which does not depend on plasma density and depends only on the reduced electric field E/p. The radial distribution of plasma density is described by the Bessel function, $n(r) = n_0 J_0\left(\frac{\kappa r}{R}\right)$. For the simplest boundary condition, n(R) = 0, one obtains $\kappa \approx 2.4$. The plasma density on the axis, n_0 , is proportional to the discharge current.

We will show that the kinetic model of electrons provides a much richer and more exciting picture of plasma behavior than the ambipolar Schottky model. We use a simplified three-level model of an argon atom with one metastable state (index m),

| Name | Reaction | Energy (eV) | Value |
|---------------------|----------------------------------|------------------------------|--|
| Elastic scattering | $e + Ar \rightarrow e + Ar$ | | Cross section |
| Excitation | $e + Ar \rightarrow e + Ar_m$ | $\varepsilon_1 = 11.5$ | Cross section |
| Super elastic | $e + Ar_m \rightarrow e + Ar$ | _ | Cross section |
| Direct ionization | $e + Ar \rightarrow 2e + Ar^+$ | $\varepsilon_{\rm i} = 15.8$ | Cross section |
| Recombination | $e + Ar^+ \rightarrow Ar$ | _ | $\sigma = 5 \times 10^{-20} \mathrm{m}^2$ |
| Stepwise ionization | $e + Ar_m \rightarrow 2e + Ar^+$ | $\varepsilon_{\rm s} = 4.3$ | Cross section |
| Penning ionization | $2Ar_m \to e + Ar^+ + Ar$ | _ | $k_{\rm P} = 1.2 \times 10^{-15} \mathrm{m}^3 \mathrm{s}^{-1}$ |

Table 1. The set of reactions for argon plasma (adapted from [21]).

considering seven main reactions listed in table 1. The constants of the electron-induced processes are computed using the corresponding collision cross-sections. The ion mobility and diffusion are $\mu_{\rm i}=0.115\frac{{\rm m}^2}{{\rm V}_{\rm S}}\frac{{\rm Torr}}{p}$ and $D_{\rm i}=\frac{\mu_{\rm i}T_{\rm i}}{e}$. The simplified model of Ar plasma neglecting the excita-

The simplified model of Ar plasma neglecting the excitation of higher atomic levels followed by radiation losses may lead to overestimating the metastable density and overestimating the gain of electron energy in superelastic collisions and Penning ionization [20]. Therefore, the respective structures in the EEDF, particularly in the dynamic range, may be affected. However, we do not expect these to change significantly the overall picture described in the present paper.

The boundary conditions for the electron kinetic equation are specified as follows. First, the energy range $u_{\rm max}$ is selected to be sufficiently large to assume $f_0\left(r,u=u_{\rm max}\right)=0$. The boundary condition at u=0

$$\frac{\partial f_0}{\partial r} - E \frac{\partial f_0}{\partial u} \to 0 \tag{17}$$

corresponds to the absence of electron flux at zero kinetic energy. The boundary condition at r = R is:

$$-\frac{\partial f_0}{\partial r} = \frac{3}{2\lambda} d\Omega f_0 \tag{18}$$

where $d\Omega$ is an effective loss cone [22, 23]. In our simulations, we used $d\Omega = 1$.

The boundary conditions for the ion drift-diffusion equation and metastable continuity equation at r = R are:

$$D_{\rm i}\frac{\partial n_{\rm i}}{\partial r} + \mu_{\rm i} E_{\rm r} n_{\rm i} = \frac{n_{\rm i}}{4} \sqrt{\frac{8T_{\rm i}}{\pi M}}$$
 (19)

$$D_{\rm m} \frac{\partial n_{\rm m}}{\partial r} = \frac{n_{\rm m}}{4} \sqrt{\frac{8T_{\rm m}}{\pi M}}.$$
 (20)

The coupled set of the FP kinetic equation for electrons, the drift-diffusion for ions, continuity for metastables, and the Poisson equation for the electric field was solved using COMSOL [24] with an implicit backward differentiation formula (BDF) time-stepping method. A direct multifrontal massively parallel sparse direct solver(MUMPS) solver was employed at each time step for all quantities. Logarithmic formulations were used for the Fokker–Planck equation for electrons, the drift-diffusion equation for ions, and the diffusion equation for metastables.

3. Results of simulations

The spatially nonlocal electron kinetics $(f_0(u,r) \neq f_0^0(u) n_e(r))$ under conditions of temporal nonlocality $(f_0(t,u) \neq f_0^0(u) n_e(t))$ are analyzed. A range of gas pressures and AC frequencies are chosen to achieve these conditions. The corresponding range of pR for the positive column corresponds to $\lambda < R < \lambda_u$, where λ_u is the electron energy relaxation length, a function of electron kinetic energy: $\lambda_u(u) = \lambda(u)/\sqrt{\delta}$ at $u < \varepsilon_1$ and $\lambda_u^*(u) = \sqrt{\lambda(u)}\lambda^*(u)$ at $u > \varepsilon_1$. Here $\lambda(u)$ is the electron mean free path at kinetic energy u, $\delta = \sqrt{2m/M}$ is the fraction of energy transferred in quasi-elastic collisions, and $\lambda^*(u)$ is the electron mean free path for inelastic collisions at the kinetic energy u. The AC angular frequency range is $\tau_a^{-1} < \omega < \nu_u$, where $\tau_a = \frac{R^2}{D_a}$ is the ambipolar diffusion time, $D_a = \frac{\mu_i T_e}{e}$, and $\nu_u(u) = \nu(u) \delta + \nu^*(u)$ is the electron energy relaxation frequency.

Figure 1 shows the characteristic frequencies (a) and lengths (b) for argon pressure of 1 Torr and tube radius of R=1 cm. The bounds on the driving frequency for the dynamic regime are determined by the inverse of the ambipolar diffusion time, τ_a^{-1} (red), as well as the energy relaxation frequency ν_u . The lower bound on the product pR is determined by the condition that the electron mean free path λ (red) is smaller than the tube radius R. For the typical electron temperature, $u=\tilde{T}_e=3\,\mathrm{eV}$, the cyclic frequency range $f=\omega/2\pi$ corresponding to the dynamic regime is approximately $1-10\,\mathrm{kHz}$. The conditions of spatial nonlocality are in the pR range from 0.1 cm Torr to 10 cm Torr.

3.1. The base case

All simulations are performed for a radius of $R=1\,\mathrm{cm}$ and AC with an amplitude $I_0=10\,\mathrm{mA}$. The base case corresponds to the gas pressure of $p=1\,\mathrm{Torr}$, and the driving frequency, f, in the range from $10^2\,\mathrm{to}\,10^5\,\mathrm{Hz}$. Simulations started with a seed electron density of $10^9\,\mathrm{cm}^{-3}$ and allowed to run until reaching a periodic steady state, i.e. $(f_0(t)=f_0(t+2\pi/\omega))$. After reaching the periodic steady state, the parameters of the positive column are recorded and analyzed.

Figure 2 shows temporal variations of the wall potential, the axial electric field, electron density, and electron temperature on the axis (r = 0) for one period at different frequencies. The discharge is in a quasi-static regime at the lowest frequency

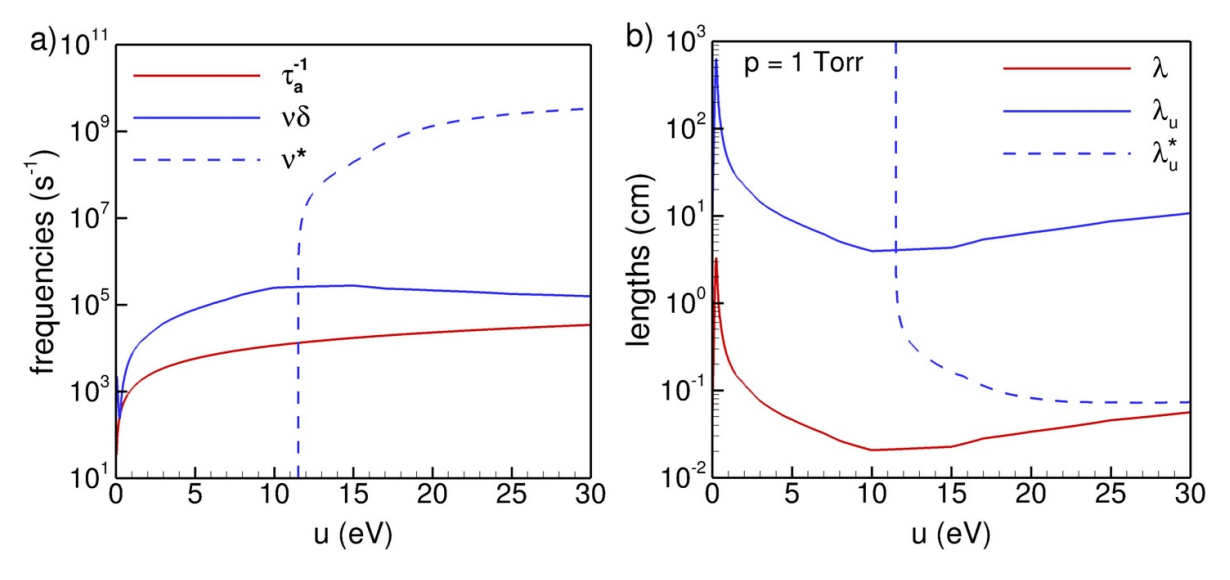


Figure 1. Characteristic frequencies (a) and lengths (b) as functions of electron kinetic energy in argon at pressure p of 1 Torr and tube radius R = 1 cm.

of 0.1 kHz. In this regime, the electric field and electron temperature remain nearly constant during most of the period, and the plasma density follows in phase with the modulation of the current. Drastic changes of all plasma parameters occur only during a short period when the current passes zero. The electron temperature drops below 0.5 eV during this short time, and the electric field and electron temperature exhibit an overshot. Substantial asymmetry of the temperature variation with time occurs when the electric field crosses zero. The temperature drops smoothly when the field amplitude decreases and increases sharply when the amplitude increases. With increasing frequency, the region of drastic changes near zero current grows relative to the AC period.

At 3 kHz, the discharge operates in the dynamic regime. The amplitude of all oscillations is lower compared to the quasi-static case. There is an extended region where the axial electric field, E_z , is close to zero. The asymmetry of the temperature profile remains substantial. Electron heating during the field rise is noticeably faster than the temperature drop during its decrease. Penning ionization helps maintain plasma when ionization by electron impact becomes small.

At 30 kHz, the driving frequency is substantially above the inverse of the ambipolar diffusion time, so the density oscillations become small. As a result, the electric field oscillations follow the current variations. The changes in electron temperature, ionization, and excitation rates (not shown) remain substantial. As the driving frequency becomes comparable to the collisional relaxation time, the variations of electron temperature decrease, and the average electron temperature is near the value in the quasi-static case (f = 0.1 kHz). The observed behavior resembles the previously obtained for ICP using a fluid plasma model [8].

The contribution to the total ionization source rate for all three driving frequencies primarily comprises stepwise and Penning ionization. Figure 3 shows the time evolution of different ionization and volume loss channels. Stepwise ionization is the main ionization channel over the period. However, Penning ionization becomes essential near zero current. The volumetric recombination is negligible at 1 Torr, and surface recombination is the main channel of particle loss.

The root mean square (rms) electric field, $\bar{E}_z = \sqrt{\langle E_z^2 \rangle}$, electron temperature, $\langle T_e \rangle$, and electron density, $\langle n_e \rangle$, are shown in figure 4. At driving frequencies below 1 kHz, all three vary relatively weekly with driving frequency. For higher frequencies, a dip in $\langle T_e \rangle$ and a maximum in $\langle n_e \rangle$ occur near 3 kHz. The obtained minimum of $\langle T_e \rangle$ in the dynamic regime agrees with previous experimental observations in discharges driven by modulating currents [2]. The observed minimum of $\langle T_e \rangle$ in [2] occurs at a frequency a factor of 3–5 larger than that observed in the present work. This difference can be due to the different masses of argon and helium studied in [2].

Figures 5–7 show the variations of the EEPF, $f_0(u,t)$, on the tube axis at frequencies 0.1, 3, and 30 kHz. At low frequency, 0.1 kHz, the shape of the EEPF remains approximately the same for most of the period, except when the current crosses zero. When the current crosses zero, the EEPF shape changes sharply (figure 5).

At 3 kHz, the shape of the EEPF varies substantially over the period (figure 6). At low currents, the EEPF becomes non-monotonic. Unlike 0.1 kHz, this non-monotonic shape remains for most of the period. The first of the two local maximums is a result of Penning ionization. The second is a result of superelastic collisions. Both of these processes occur as the number density of metastables remains substantial during the portion of the period where electron temperature becomes low.

Finally, at 30 kHz, the variations of the EEPF shape are significantly reduced (figure 7). At this frequency, the electron number density varies slightly, but the variations in electron temperature remain substantial. The EEPF is a monotonic function of kinetic energy at 30 kHz.

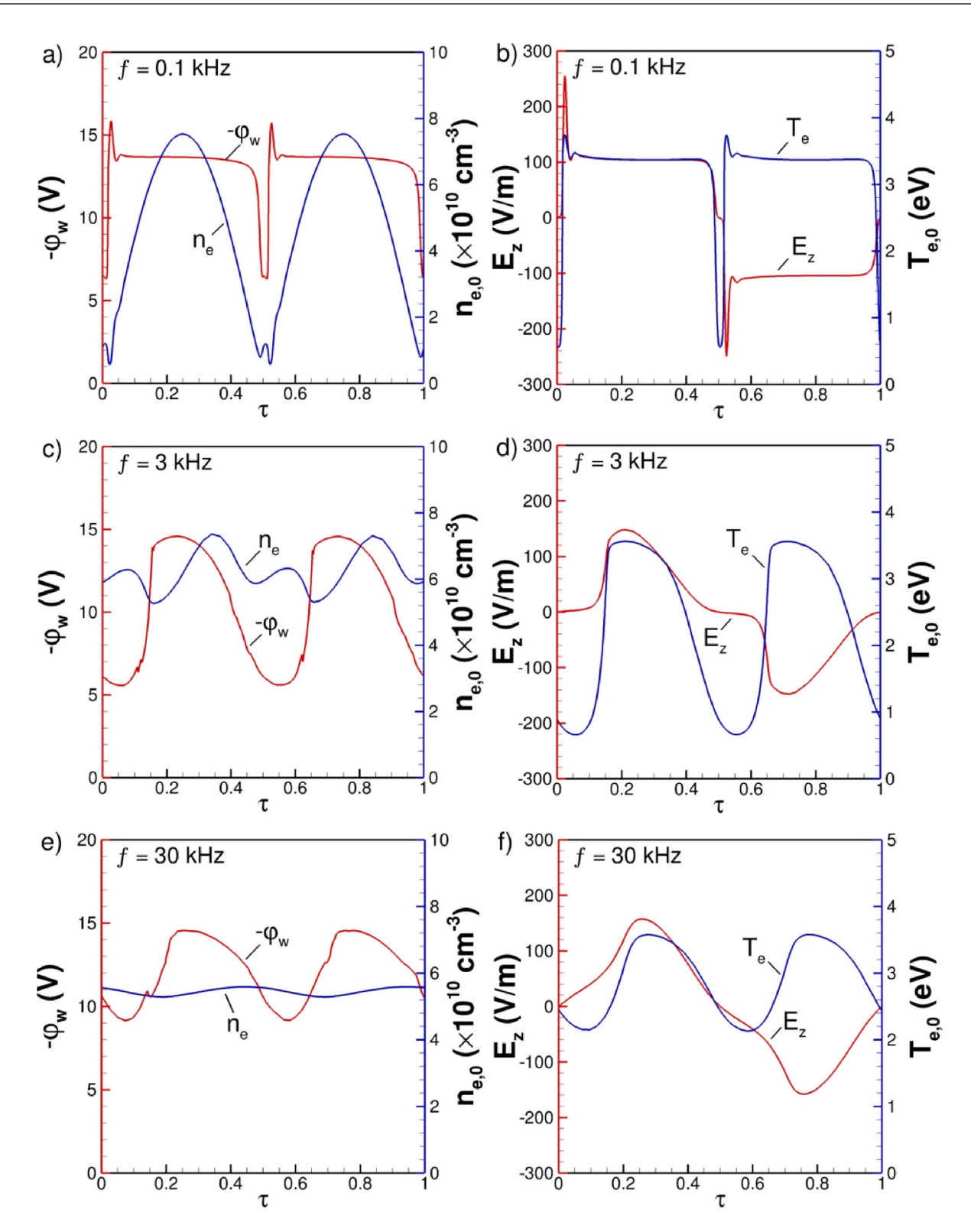


Figure 2. Temporal variations of the wall potential and electron density (left) and electric field and electron temperature (right) at the tube center for frequencies f = 0.1, 3, and 30 kHz.

3.2. The pressure dependence

We have conducted simulations at f = 3 kHz for different p in the range 0.1–10 Torr. Figures 8–10 show the radial distributions of electron density (a), metastable density (b), electron temperature (c), and ionization rate (d) over one period for

pressures of 3, 6, and 10 Torr. At p = 3 Torr, the radial distributions of electron and metastable densities, electron temperature, and ionization rate are monotonic. Moderate radial constriction occurs for the metastable density due to stepwise ionization (dotted line in figure 8(d)).

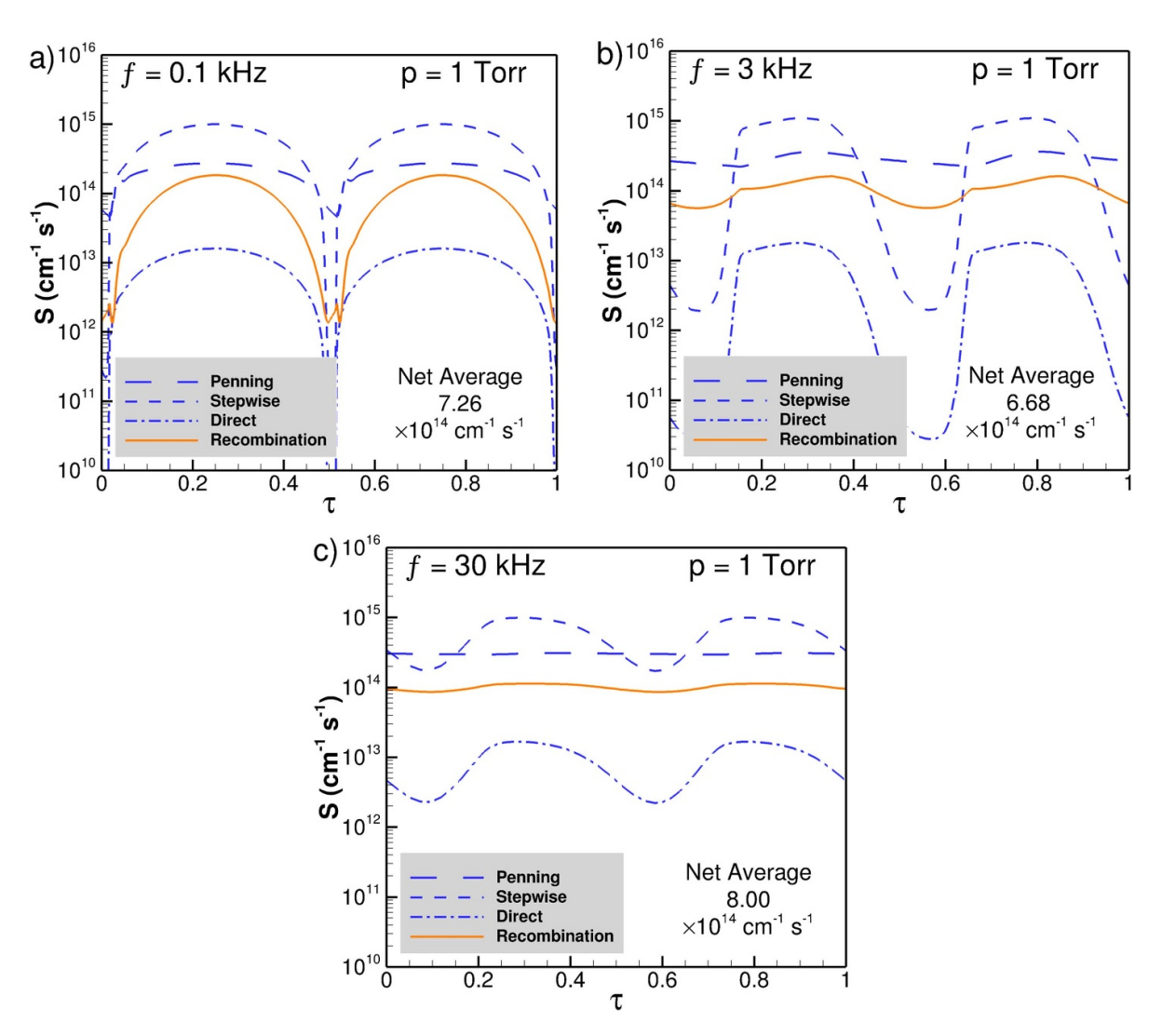


Figure 3. The rates of Penning, stepwise, and direct ionization as functions of time during the AC period. The loss rate is due to surface recombination.

At p=6 Torr, an off-axis peak of plasma density forms (figure 9). Steep off-axis maxima of metastable density and stepwise ionization rate are also present. The maximum plasma density peak relative to the tube center occurs near the maximum current ($\tau=0.25$). At zero current ($\tau=0$), the plasma density nears, but does not become, monotonic.

At p = 10 Torr, the plasma density peak is located closer to the wall and is more pronounced (figure 10). A pronounced off-axis maximum plasma density (\sim 20% greater than the axial value) remains throughout the period. Additionally, a 'spike' in electron temperature near the wall occurs near the current zero. This spike is most pronounced at the highest pressure (p = 10 Torr) studied in the present paper.

Figure 11 compares the dependence of the reduced electric field E/p on the reduced frequency f/p for varying pressure at f=3 kHz (in red) and varying frequency at p=1 Torr (in green). The f/p scaling is not satisfied in our model. A much stronger dependency on pressure observed in our simulations

may be due to Penning ionization. Further studies of the f/p scaling could be the subject of additional studies.

4. Peculiarities of the dynamic regime of discharge operation

The dynamic regime of plasma operation becomes possible due to the significant difference in the ambipolar diffusion time, τ_a , and the electron energy relaxation time, τ_u . This disparity of time scales is a consequence of the small electron mass compared to the ion mass. In our studies, τ_u is shorter than τ_a by two orders of magnitude. The peculiarities of plasma dynamics in the frequency range $\tau_u \ll \omega^{-1} \ll \tau_a$ have been previously studied in [8] using a fluid model for electrons. In the dynamic regime, the plasma density varies slightly over the AC period, but the electron temperature, ionization rate, and the EEDF shape change significantly. This

10¹⁰

10²

τ

0.125

0.4375

0.5625

0.5

15

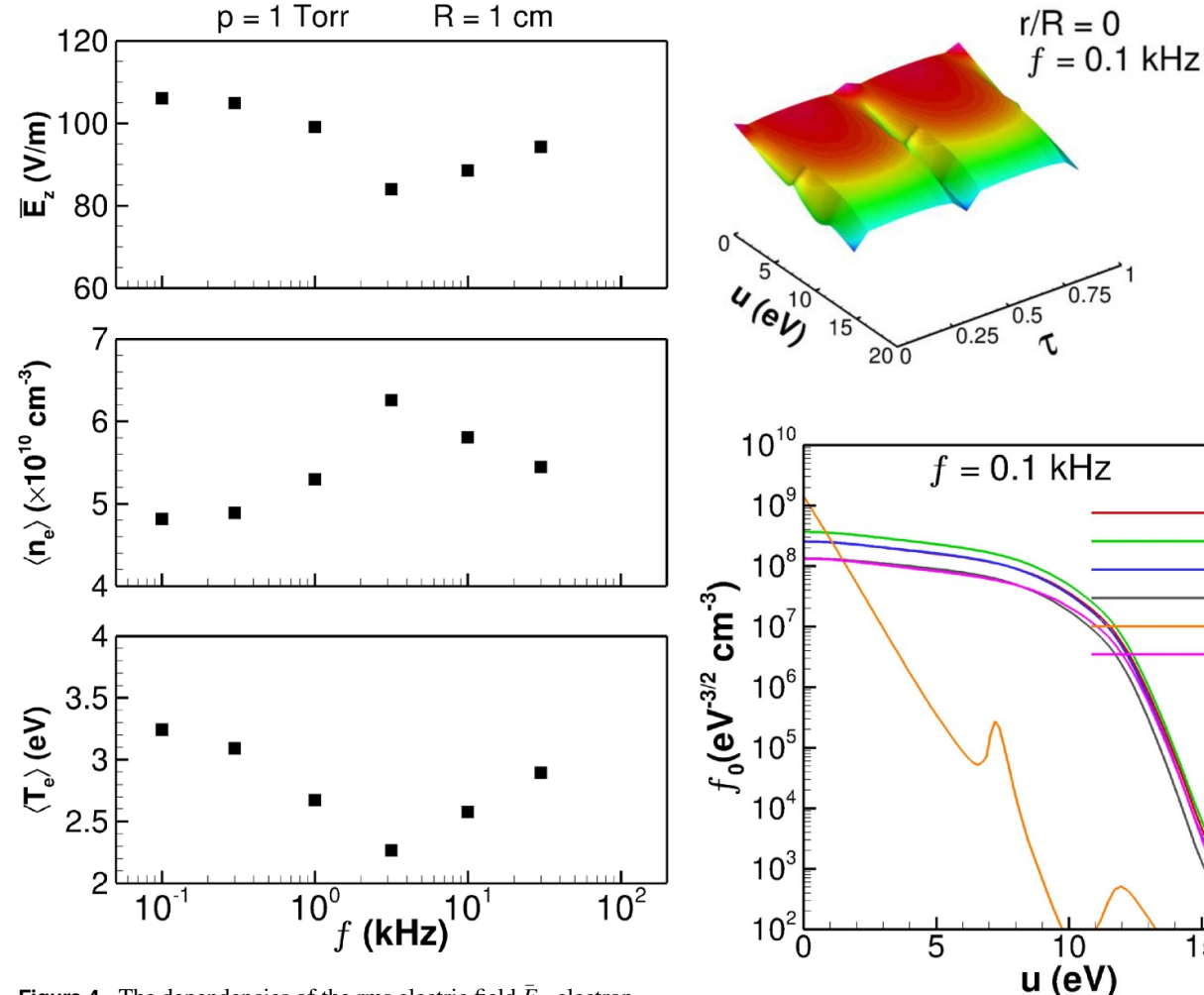


Figure 4. The dependencies of the rms electric field \bar{E}_z , electron density $\langle n_e \rangle$, and electron temperature $\langle T_e \rangle$ at the tube axis on driving frequency f, for p = 1 Torr.

operating regime has found application in fluorescent lamps driven at 20-100 kHz [25].

4.1. Increased efficiency of plasma maintenance in the dynamic regime

Figure 12 illustrates the origin of the increased efficiency of plasma maintenance in the dynamic regime. In a positive column, the number of ionizations must be equal to the number of electron losses over the AC period:

$$\int_{0}^{T} \nu_{i}(t) dt = \int_{0}^{T} \tau_{a}^{-1}(t) dt$$
 (21)

This condition defines the electric field and the mean electron energy u_0 required to maintain the plasma. In particular, equation (21) defines a specific value of the electric field E_0 in DC discharges.

In AC discharges, the axial electric field changes sign oscillating during the current period. However, substantial modulations of the mean electron energy (temperature) occur only in a

Figure 5. The EEPF, $f_0(u)$, as function of kinetic energy six times during an AC period at f = 0.1 kHz.

limited frequency range corresponding to the dynamic regime. At high frequencies, $f \gg \tau_u^{-1}$, modulations of electron temperature vanish, and the mean value of the temperature depends on the effective value of the electric field, $E_0/\sqrt{2}$, defined by equation (21).

Due to the nonlinear dependence of the ionization rate, $\nu_i(u)$, on the electron energy (see figure 12), time modulations of the electron kinetic energy produce more ionizations during the period than required to balance losses that scale linearly with electron kinetic energy. Thus, to maintain the balance, the rms electric field and the mean electron temperature must be smaller, and the efficiency of plasma maintenance must be higher in the dynamic regime.

4.2. Nonlocal kinetic effects in the dynamic regime

Several assumptions of the fluid model discussed above become invalid when nonlocal effects are essential. First, the EEDF cannot be factorized as $f_e(u, r) \neq f_0(u) n_e(r)$, which can be termed spatial nonlocality. Second, the EEDF cannot be

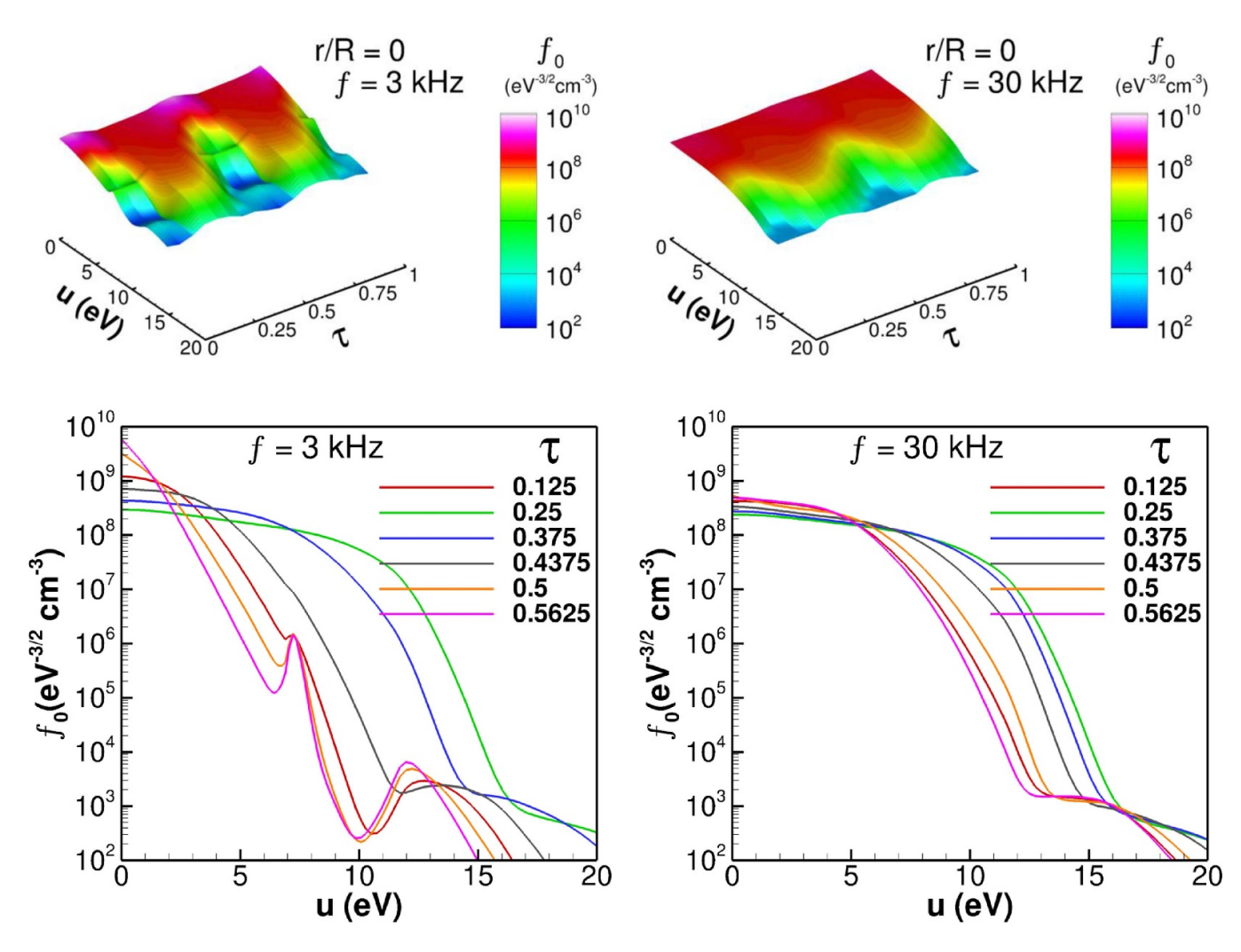


Figure 6. The EEPF, $f_0(u)$, vs kinetic energy at six times during one AC period at f = 3 kHz.

Figure 7. The EEPF, $f_0(u)$, vs kinetic energy at four times during a half AC period at 30 kHz.

factorized as $f_e(u,t) \neq f_0(u) n_e(t)$, which can be termed *temporal* nonlocality. In low-pressure AC discharges operating in dynamic regimes, both spatial and temporal nonlocality play a role $f_e(u,r,t) \neq f_0(u) n_e(r,t)$. As illustrated in the present paper, nonlocal electron kinetics produces exotic effects in the dynamic regime.

As discussed in [1], the energy relaxation times and lengths are strikingly different for the EDF body and tail. For the EDF tail $(u > \varepsilon_1)$ the characteristic time is $1/\nu^*$ and the energy relaxation length can be estimated as

$$\lambda_u^* = \sqrt{D_r/\nu^*} = \sqrt{\lambda \lambda^*} \sim (3 - 10)\lambda. \tag{22}$$

The characteristic time τ_f of the EEDF body relaxation at $u < \varepsilon_1$, depends on the overall energy balance of electrons. At elevated gas pressures (pR > 1 cm Torr), energy loss in quasi-elastic collisions controls the electron energy balance, $\tau_f \sim \tau_u = \frac{1}{\delta \nu}$. This time of the EEDF body relaxation is much longer than the corresponding time for the tail relaxation.

At low gas pressures (pR < 1 cm Torr), when inelastic collisions control the energy balance of electrons, the characteristic time τ_f of the EEDF's body relaxation is much longer than the time $\tau_E = \frac{1}{\nu_E} = \varepsilon_1^2/D_E$, that is required for electrons to diffuse from zero energy to the excitation energy ε_1 . The corresponding length is

$$\lambda_E = \sqrt{D_r \tau_E} = \varepsilon_1 / (eE). \tag{23}$$

During the time τ_E , quasi-elastic energy losses are small because $\tau_E < \tau_u$. The asymmetry of the electron temperature in AC discharges during the transit over zero current is a consequence of different cooling and heating rates. When the amplitude of the electric field decreases, the EEDF relaxation occurs slowly over the time $\tau_f \sim \frac{1}{\delta \nu}$ (this prevents the electron temperature from dropping to the gas temperature). When the amplitude of the electric field increases, the EEDF formation occurs much faster with the characteristic time $\tau_E < \frac{1}{\delta \nu} = \tau_u$. This asymmetry was previously observed in simulations in

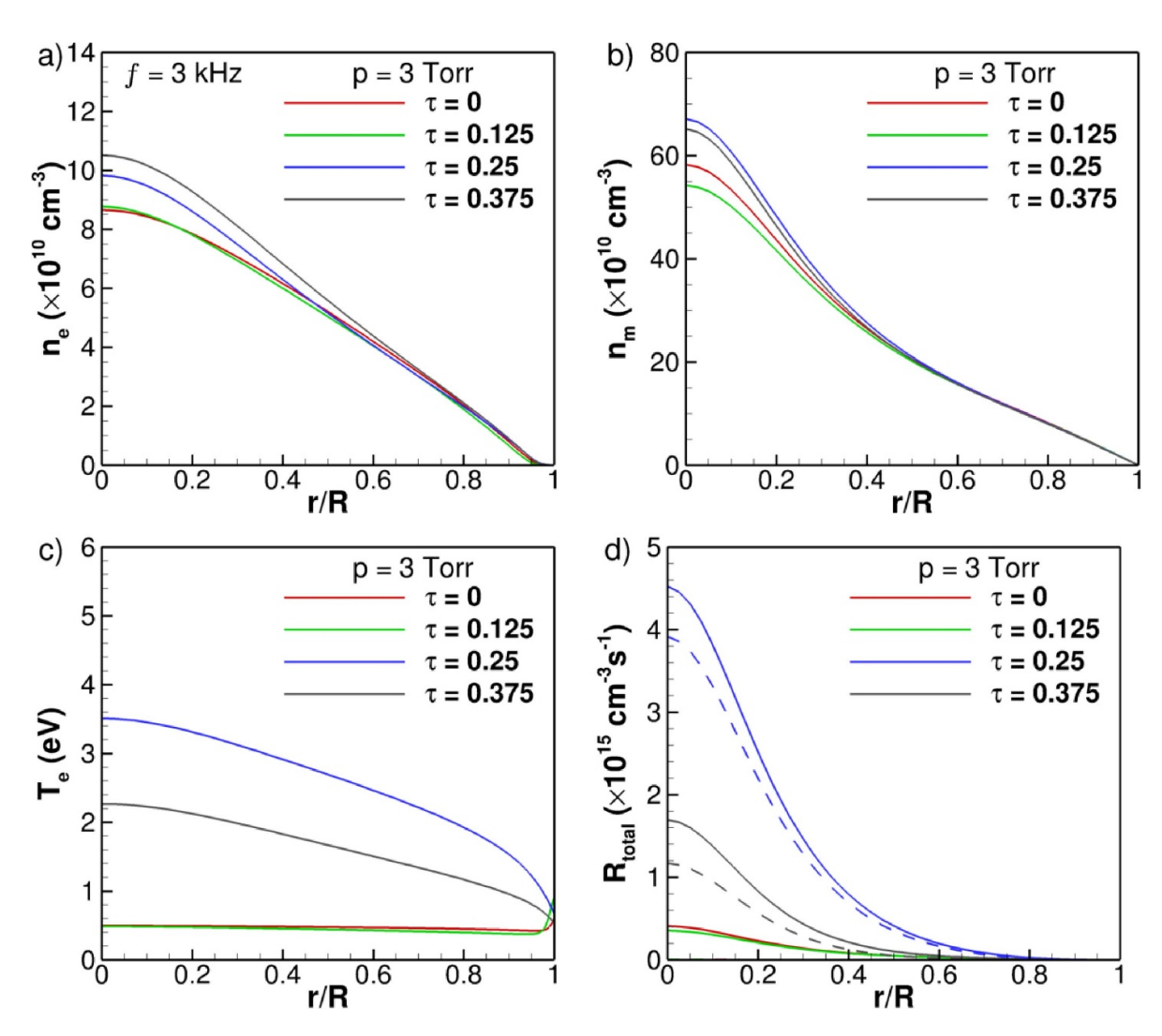


Figure 8. Radial distributions of electron density (a), metastable densities (b), electron temperature (c), and ionization rates (d) four times throughout half a period for pressure p = 3 Torr. Dashed lines in the distribution of ionization rates show the contribution from stepwise ionization.

Neon [26] and was discussed in the book [1] for spatially uniform plasma.

4.3. The total energy viewpoint

Peculiarities of nonlocal electron kinetics in the dynamic regime can be best illustrated using the *total* energy approach. Using total energy $\varepsilon = u - \varphi(r,t)$ as an independent variable, we can rewrite equation (8) in the form:

$$\frac{\partial f_0}{\partial t} - \frac{\partial \varphi}{\partial t} \frac{\partial f_0}{\partial \varepsilon} - \frac{1}{vr} \frac{\partial}{\partial r} \left(rv D_r \frac{\partial f_0}{\partial r} \right) - \frac{1}{v} \frac{\partial}{\partial \varepsilon} \left(v \Gamma_u \right) = S_0^*. \tag{24}$$

The speed $v(r, \varepsilon(t))$ becomes the Lame coefficient in the (r, ε) space.

The transition to the total energy corresponds to the diagonalization of the diffusion tensor (7). Although the

transition to total energy simplifies the kinetic equation (8) by removing the cross-derivative terms, it makes the integration domain $v(r,\varepsilon,t)>0$ for equation (24) more complicated and time-dependent [27]. Equation (8) is preferable for the numerical solution, as discussed in [16]. However, the total energy viewpoint is more transparent in understanding the simulation results.

Many publications have used the total energy approach to analyze electron kinetics in gas discharges (see [28, 29] and references therein). Equation (24) coincides with the heat conduction equation in a thermo-isolated flexible bag bounded by the curve $v(r,\varepsilon,t)=0$ and $\varepsilon=\varphi_{\rm w}$ (the top of the bag). The heat can escape to the wall (r=R) only above the bag top, at $\varepsilon>\varphi_{\rm w}$. The second term in equation (24) describes the effect of the bag shape changes. Electron production in the ionization events corresponds to the heat release at the bottom of the bag. Excitations of the atomic levels by electron impact produce a heat sink at the top of the bag, and the corresponding

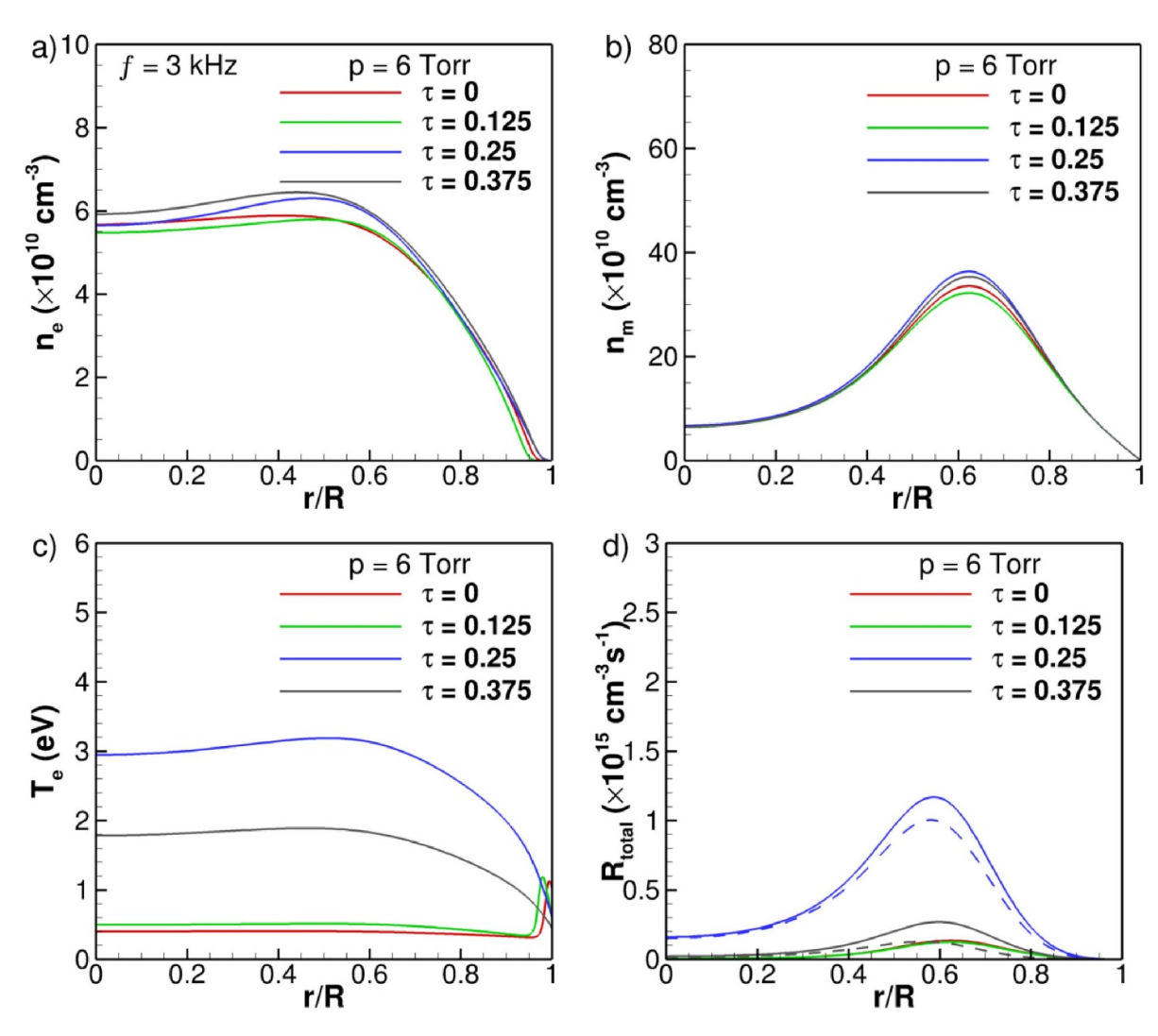


Figure 9. Radial distributions of electron density (a), metastable densities (b), electron temperature (c), and ionization rates (d) for four times throughout half a period at p = 6 Torr. Dashed lines in the distribution of ionization rates show the contribution from stepwise ionization.

heat release at the bottom, as described by the right-hand side of (24). The excitations do not change the total heat amount in the bag as the hot electrons disappear, and the same number of cold electrons reappear at the bottom.

The heat conduction analogy helps illustrate different scenarios of the EEDF formation depending on pR values. At low values of pR, when the electron energy loss in elastic collisions is negligible, the EEDF of trapped electrons (with $\varepsilon < \varphi_w$) depends only on the total electron energy and does not depend explicitly on the spatial coordinate r [30]. Figure 13 demonstrates that the total energy scaling is perfectly satisfied in our simulations at low pressure, whereas the EEPF depends explicitly on the radial position at high pressure. Indeed, at p=0.1 Torr (figure 13(a)), the relaxation length is sufficiently large compared to the tube radius for both low and high-energy electrons. The EEPF body and tail are functions of total electron energy. With increasing pR, the explicit dependence of the radial position first appears in the tail, as was observed in our

simulations at 1 Torr (see the base case above). With a further increase of pR, the entire body starts depending on the kinetic rather than total energy. Figure 13(b) illustrates this effect for p = 10 Torr.

Additional deviations from the total energy behavior can occur in AC discharges when the first two terms in equation (24) become essential. Figure 14 shows the EEPF plotted as a function of the total energy at maximum and zero currents. For 0.1 kHz (top part of figure 14), the body of EEPF is a function of the total energy, but its tail depends explicitly on the radial coordinate (because $\lambda_u^* < R$ for $pR \sim 1$). The tail is most depleted by the fast electrons near the axis due to the loss of these electrons in inelastic collisions. Therefore, the spatial component of electron flux in phase space (see the section below) must be directed toward the axis at these energies. Near zero current ($\tau = 0$), the body is a function of the total energy except for the two peaks, which depend on the radial position. The first peak

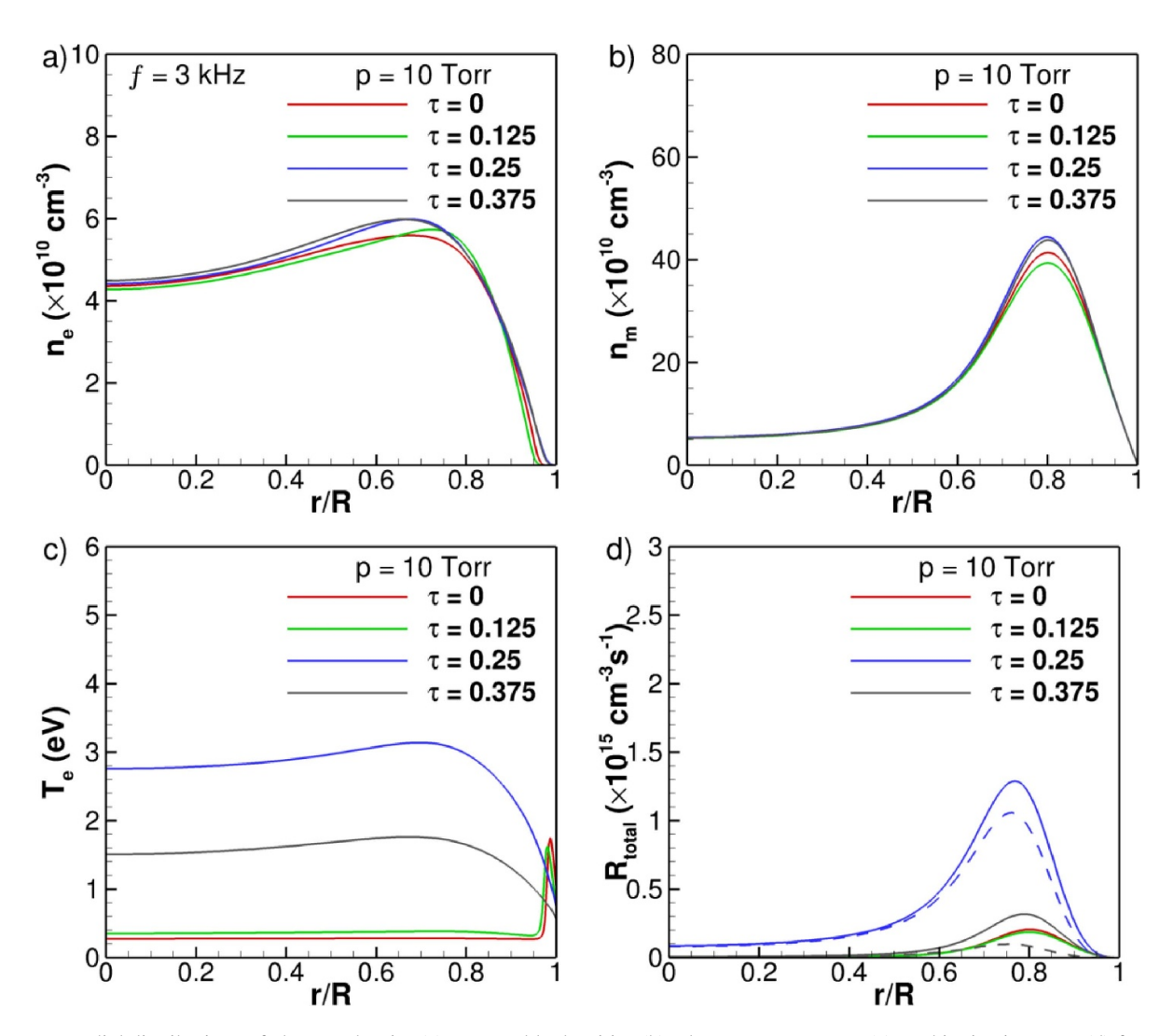


Figure 10. Radial distributions of electron density (a), metastable densities (b), electron temperature (c), and ionization rates (d) four times throughout half a period at p = 10 Torr. Dashed lines in the distribution of ionization rates show the contribution from stepwise ionization.

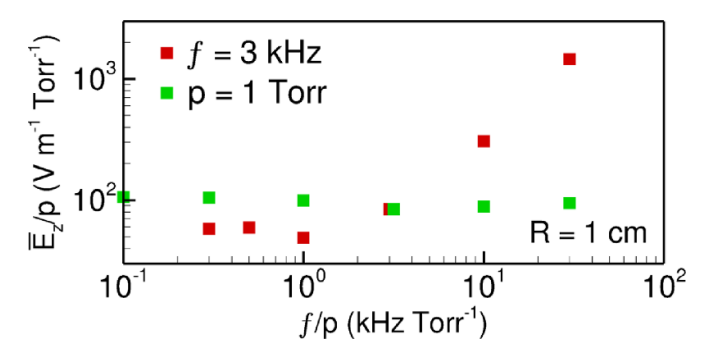


Figure 11. Reduced electric field E/p vs. f/p by varying pressure at 3 kHz (in red) and varying frequency at 1 Torr (in green).

at the energy of about 7 eV is due to the electrons generated by Penning ionization. The second peak at the energy of about 12 eV is associated with superelastic collisions and is proportional to the low-energy part (body) of the EEPF [31].

At f=3 kHz (middle part of figure 14), the picture is qualitatively similar. Throughout the period, explicit radial dependence occurs only at high electron energies (above ~ 10 eV). At f=30 kHz (bottom part of figure 14), the EEPF at maximum current looks similar to the previous cases, but the EEPF near current zero lacks the peaks present at lower driving frequencies. The electrons have insufficient time to cool down at this frequency when the electric field $E_z(t)$ crosses zero.

4.4. Electron fluxes in phase space

The formation of electron fluxes in phase space for a DC positive column under nonlocal conditions has been discussed in several publications [7, 22, 23, 30]. This section discusses the peculiarities of electron fluxes in phase space in the dynamic regime. The kinetic equation (24) can also be written as:

$$\frac{\partial f_0}{\partial t} - \frac{\partial \varphi}{\partial t} \frac{\partial f_0}{\partial \varepsilon} + \frac{1}{vr} \frac{\partial}{\partial r} (rv\Phi_r) + \frac{1}{v} \frac{\partial}{\partial \varepsilon} (v\Gamma) = S_0.$$
 (25)

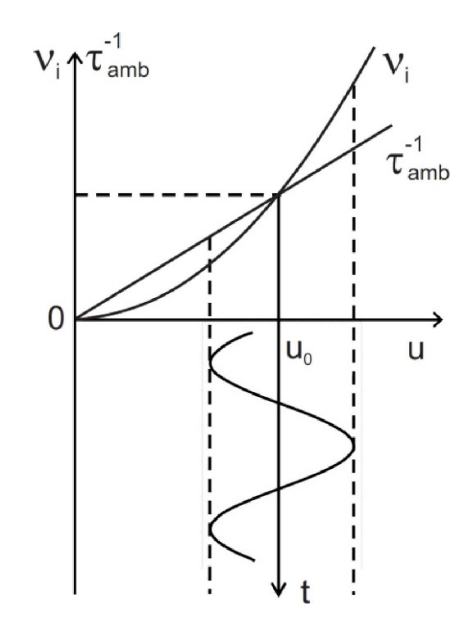


Figure 12. Illustration of enhanced ionization by the time modulation of the electric field due to nonlinear dependence of the ionization frequency on the field strength. Adapted with permission from [3].

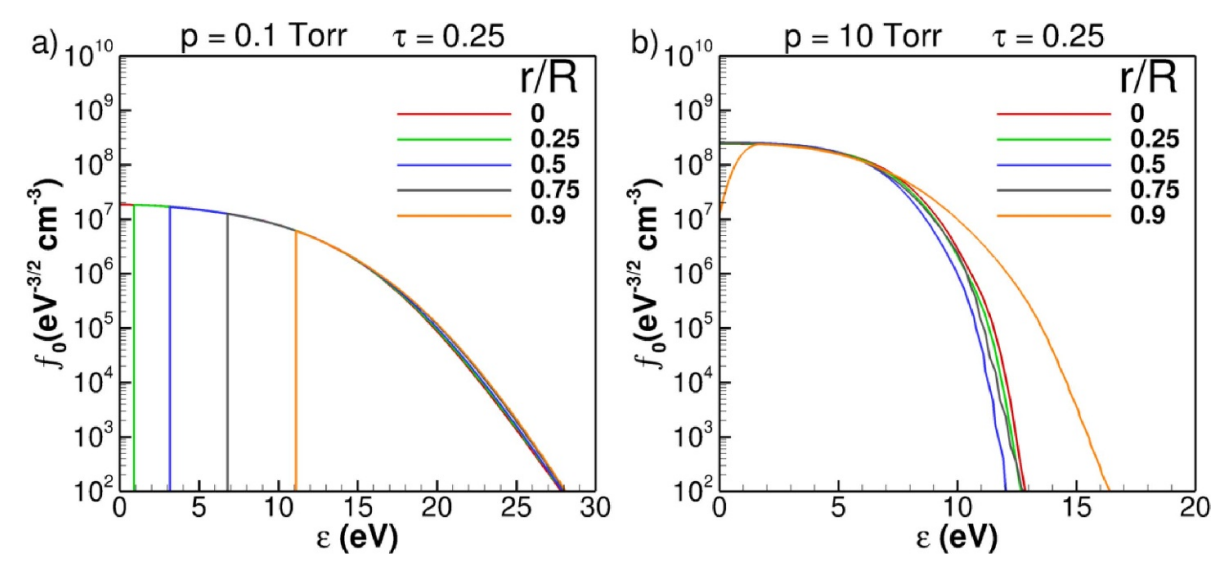


Figure 13. The EEPF at different radial positions as a function of total energy for 0.1 Torr (a) and 10 Torr (b) at a peak current ($\tau = 0.25$) for f = 3 kHz.

The electron fluxes in (r,ε) phase space are simplified compared to fluxes (4,5) in (r,u) phase space:

$$\Phi_r = -D_r \frac{\partial f_0}{\partial r} \tag{26}$$

$$\Gamma = -\Gamma_u. \tag{27}$$

The spatial flux Φ_r must be zero on the axis where $\frac{\partial f_0}{\partial r}=0$ and also at the boundary $v(r,\varepsilon,t)=0$, which reflects electrons with the total energy $\varepsilon<\varphi_{\rm w}(t)$. At $\varepsilon>\varphi_{\rm w}(t)$, the spatial flux Φ_r describes electrons escaping to the wall in a process called diffusive cooling. The energy flux Γ consists of the

diffusion (heating) component directed upwards and the convection (cooling) component directed downward.

Figure 15 shows an example of flux distributions in phase space (r,ε) for different driving frequencies, at three times during the period for 1 Torr. Under these conditions, the energy loss in the elastic collisions is negligible, and the flux Γ is directed upwards during most of the AC period. The exception to this behavior appears near the tube center at energies about $\varepsilon/\varepsilon_1\approx 0.7$ at times $\tau=0.25,0.375$, where a net downward flux in energy results in a vortex formation in phase space. The radial flux of fast electrons is directed toward the axis, which is consistent with figure 12, where the number of fast electrons is depleted near the center due to inelastic collisions at $\lambda_u^* < R$ for $pR \sim 1$.

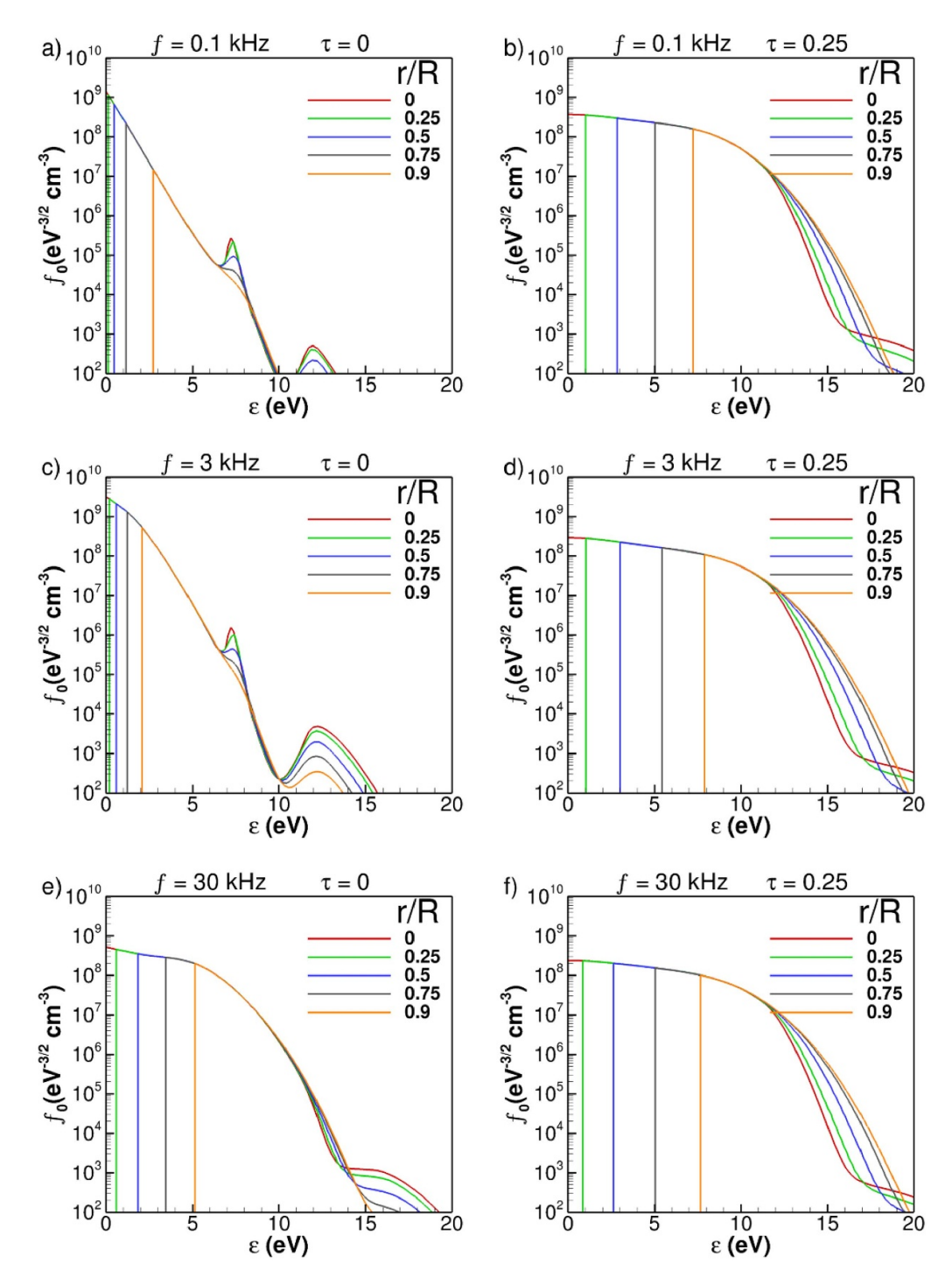


Figure 14. The EEPF as a function of total energy, $f_0(\varepsilon)$, at maximum ($\tau = 0.25$) and zero ($\tau = 0$) currents for f = 0.1, 3, 30 kHz, p = 1 Torr.

As seen in figure 2, the wall potential $\varphi_{\rm w}(t)$ drops below the excitation energy threshold ε_1 when current is zero ($\tau=0$). The energy fluxes at this time (figure 15, bottom row) are solely from losses in elastic collisions (via V_u term). At the two smaller frequencies, 0.1 and 3 kHz, $\varphi_{\rm w}(t)$ drops far below ε_1 at $\tau=0$, and strong radial fluxes are formed across the tube due to escape to the wall of electrons with $\varepsilon>\varphi_{\rm w}(t)$.

The electron fluxes in phase space (r,ε) in the dynamic regime may contain a normal component at the boundary u=0 and the streamlines originating or terminating at the boundary u=0. This behavior becomes possible because of the moving boundary $u(r,\varepsilon,t)=0$, and should be most pronounced near the current zero when the radial potential profile $\varphi(r,t)$ changes rapidly. This effect did not appear in previous

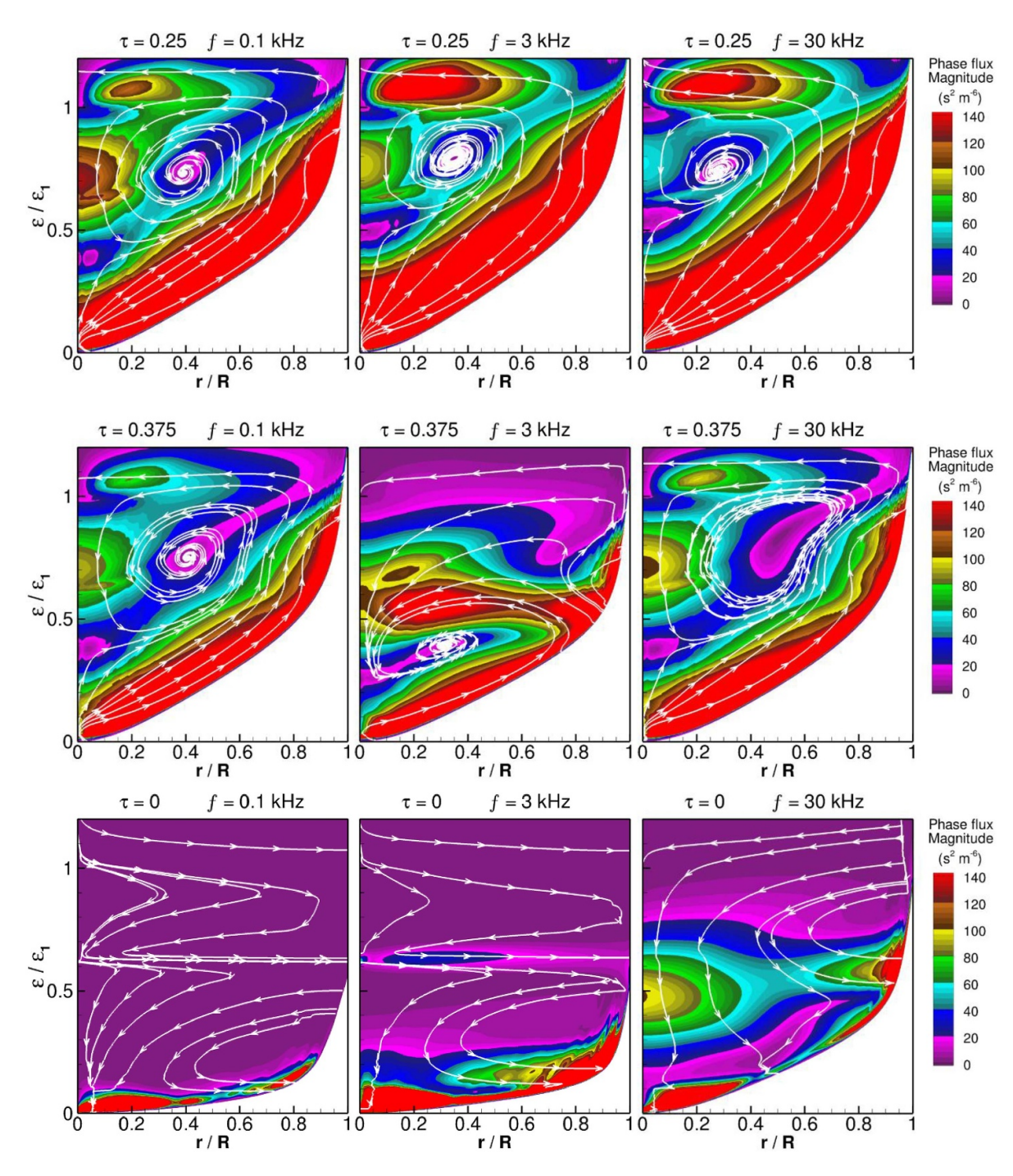


Figure 15. Electron flux magnitude (color) and streamlines in phase space at times $\tau = 0.25$ (top row), 0.375 (middle row), and 0 (bottom row) for f = 0.1 (left), 3 (center), and 30 (right column) kHz.

publications devoted to studies of electron fluxes in phase space in DC discharges because in steady-state, boundary conditions prevent streamlines in (r,ε) phase space from having a normal component at the boundary u=0. Figure 15 shows that in AC discharges, streamlines could form and terminate at the boundary u=0 (where $\varepsilon=-\varphi(r,t)$) especially at small currents. This is countered with a change in the electric potential with respect to time at this radial position (second term in equation (24)). In the dynamic regime (f=3 kHz),

this peculiar state of the fluxes at the boundary u = 0 is also observed at other times during the period.

5. Conclusions

We have performed hybrid kinetic-fluid simulations of a positive column in AC argon discharges in the collisional regimes $(\lambda \ll R)$ over various driving frequencies and gas pressures.

We have focused on the low pR conditions ($\lambda_u \gtrsim R$) when the spatial nonlocality of the EEDF is substantial. It was confirmed that the most efficient (minimal power) conditions of plasma maintenance are observed in the dynamic regime. The minimal values of a period-averaged axial electric field and the electron temperature have been observed at f/p values of about 3 kHz Torr⁻¹. The ionization rate and plasma density reached maximal values under these conditions.

The Fokker-Planck kinetic solver for EEDF was used to properly account for the nonlocal kinetic effects associated with spatial and temporal nonlocality of the EEDF. Using kinetic energy as an independent variable, we obtained an efficient solution of the anisotropic tensor diffusion equation in phase space. We clarified the role of the diagonal terms, which describe space diffusion and electron heating, and off-diagonal terms, which are responsible for the energy conservation during electron diffusion in phase space (over surfaces of constant total energy). An important conclusion worth emphasizing is that electron heating depends on the absolute value of the *local* electric field. As a result, the ambipolar electric field, which decelerates and traps electrons, contributes to electron heating on the plasma periphery (at $r \sim R$), where the amplitude of the ambipolar field exceeds the amplitude of the axial field.

We have shown that the kinetic view uncovers a more exciting and rich physics than the classical ambipolar diffusion (Schottky) model. The electron fluxes in phase space illustrate an interesting behavior under conditions of temporal and spatial nonlocality of the collisional electron transport. The electrons at different energies can flow in opposite directions. The energy component of the flux changes its direction during the AC period. The difference between the heating and cooling rates results in the asymmetry of the EEDF behavior and the time variation of electron temperature when the current passes through zero value.

We have confirmed that electron diffusion with conservation of the total electron energy is valid when the temporal variations are slow compared to the EEDF relaxation time. The EEDF under these quasi-static conditions is a function of the total energy only and depends on space and time implicitly. Deviations from this behavior have been detected during rapid variations of the electric fields near current zero when the additional transient terms in the kinetic equation become essential. The radially non-monotonic distributions of excitation rates, metastable densities, and even the plasma density have been observed in our simulations with increasing pR. The off-axis peak of the plasma density in the dynamic regime predicted by our model has never been observed in experiments. We hope our results stimulate further experimental studies of the AC positive column. The kinetic analysis could help uncover new physics even for such a well-known plasma object as a positive column in noble gases. Recent kinetic simulations of a low-pressure collisional positive column in Nitrogen DC discharges have also demonstrated an off-axis peak of the electron temperature due to electron heating by the radial ambipolar electric field [32].

A few comments regarding desired future experiments to validate our modeling predictions. Recent efforts [20] to experimentally observe the kinetic effects predicted by the theory of DC positive column in noble gases have had mixed success. The radial constriction of the light emission caused by radial decay of the high-energy tail of the EEDF and contraction of the excitation zone were experimentally observed at low pressure (0.25 Torr). A significant broadening of the light emission profiles was observed at elevated pressures, but the non-monotonic radial profile of the excitation rate was not found in the experiment. In our view, this discrepancy may be caused by moving striations in the experiments, which were not accounted for in the theory.

In radio-frequency AC discharges of noble gases, standing striations have been observed [33]. It is expected that plasma stratification could also occur in the dynamic regimes, as recently observed in atmospheric pressure dielectric barrier discharges in argon at 60 kHz [34]. So, experimental studies of the radial structure of positive columns in AC discharges should consider possible plasma stratification. For the experimental measurements of radial distributions of electron density in the dynamic regimes, bremsstrahlung intensity could be used [35].

The Knudsen regimes $(\lambda \ge R)$ of the weakly collisional positive column will be the subject of future studies.

Data availability statement

All data that support the findings of this study are included within the article (and any supplementary files).

Acknowledgments

This work was supported by the NSF Projects OIA-1655280, 2148653 and DOE Project DE-SC0021391. Nathan Humphrey thanks Dr Robert Arslanbekov for introducing him to plasma modeling and to simulations in COMSOL. The authors thank Dr Evgeny Bogdanov for sharing his experiences of plasma simulations using COMSOL.

References

- [1] Kudryavtsev A A, Smirnov A S and Tsendin L D 2010 *Physics* of *Glow Discharge* (St. Petersburg) (in Russian)
- [2] Polman J and van der Werf J E 1970 Enhanced light emission from positive column by means of current modulation Appl. Phys. Lett. 17 15
- [3] Milenin V M and Timofeev N A 1991 Plasma of Low Pressure Gas Discharge Light Sources (Leningrad Univ. Publ) (in Russian)
- [4] Barnat E V and Kolobov V I 2013 Nonmonotonic radial distribution of excited atoms in a positive column of pulsed direct current discharges in helium *Appl. Phys. Lett.* 102 034104

- [5] Arslanbekov R R, Kolobov V I, Bogdanov E A and Kudryavtsev A A 2004 Nonmonotonic excitation rates in argon positive column Appl. Phys. Lett. 85 3396
- [6] Bogdanov E A, Kudryavtsev A A, Tsendin L D, Arslanbekov R R and Kolobov V I 2004 Nonlocal phenomena in the positive column of a medium-pressure glow discharge *Tech. Phys.* 49 849
- [7] Tsendin L D, Bogdanov E A and Kudryavtsev A A 2005 Paradoxical nonmonotonic behavior of excitation-rate spatial profiles in bounded plasmas *Phys. Rev. Lett.* 94 015001
- [8] Kolobov V I and Godyak V A 2017 Inductively coupled plasmas at low driving frequencies *Plasma Sources Sci. Technol.* 26 075013
- [9] Yuan C, Bogdanov E A, Kudryavtsev A A and Zhou Z 2018 Vortex electron flux and EDF nonlocality of moderate and high-pressure gas discharge plasmas *Plasma Sources Sci. Technol.* 27 045007
- [10] Yuan C, Bogdanov E A, Kudryavtsev A A, Rabadanov K M and Zhou Z 2017 Ambipolar field role in formation of electron distribution function in gas discharge plasma Sci. Rep. 7 14613
- [11] Yuan C, Bogdanov E A, Eliseev S I and Kudryavtsev A A 2017 1D kinetic simulations of a short glow discharge in helium *Phys. Plasmas* **24** 073507
- [12] Kolobov V I, Guzman J A and Arslanbekov R R 2022 A self-consistent hybrid model of kinetic striations in low-current argon discharges *Plasma Sources Sci. Technol.* 31 035020
- [13] Shkarofsky I P, Johnston T W and Bachynski M P 1966 *The* Particle Kinetics of Plasmas (Addison-Wesley)
- [14] Gurevich A V 1978 Nonlinear Phenomena in the Ionosphere (Springer)
- [15] Kolobov V I and Arslanbekov R R 2006 Simulation of electron kinetics in gas discharges *IEEE Trans. Plasma Sci.* 34 895
- [16] Kolobov V I and Arslanbekov R R 2022 Ionization waves in low-current dc discharges in noble gases obtained with a hybrid kinetic-fluid model *Phys. Rev.* E 106 065206
- [17] Michel O, Duclous R, Masson-Laborde P-E, Enaux C and Lafitte P 2023 A nonlocal electron transport model in the diffusion scaling of hydrodynamics *Phys. Plasmas* 30 022712
- [18] Yuan C, Bogdanov E A, Kudryavtsev A A, Rabadanov K M and Zhou Z 2019 Influence of electron–electron collisions on the formation of a nonlocal EDF *Plasma Sources Sci. Technol.* 28 015001
- [19] Fu Y, Wang H and Wang X 2023 Similarity theory and scaling laws for low temperature plasma discharges: a comprehensive review Rev. Mod. Plasma Phys. 7 10

- [20] Golubovskii Y, Kalanov D, Gorchakov S and Uhrlandt D 2015 Nonlocal electron kinetics and spectral line emission in the positive column of an argon glow discharge *Plasma Sources* Sci. Technol. 24 025028
- [21] Yuan C, Yao J, Bogdanov E A, Kudryavtsev A A and Zhou Z 2020 Formation of inverse electron distribution function and absolute negative conductivity in nonlocal plasma of a dc glow discharge *Phys. Rev.* E 101 031202(R)
- [22] Alves L L, Gousset G and Ferreira C M 1997 Self-contained solution to the spatially inhomogeneous electron Boltzmann equation in a cylindrical plasma positive column *Phys. Rev.* E 55 890
- [23] Mu"mken G, Schlu"ter H and Tsendin L D 1999 Formation mechanisms of radial electron fluxes in a positive column *Phys. Rev.* E 60 2250
- [24] 2023 COMSOL Multiphysics 5.6 (available at: www.comsol. com)
- [25] Rea M S 1993 *Lighting Handbook* 8th edn (IESNA Publication) p 209
- [26] Wilhelm J and Winkler R 1979 Progress in the kinetic description of non-stationary behaviour of the electron ensemble in non-isothermal plasmas J. Phys. Colloq. 40 C7–251
- [27] Albritton J R 1983 Laser absorption and heat transport by non-Maxwell-Boltzmann electron distributions *Phys. Rev.* Lett. 50 2078
- [28] Kolobov V I and Godyak V A 2019 Electron kinetics in low-temperature plasmas Phys. Plasmas 26 060601
- [29] Tsendin L D 2010 Nonlocal electron kinetics in gas-discharge plasma Phys. Usp. 53 133
- [30] Kortshagen U and Lawler J E 1999 Energy-resolved electron particle and energy fluxes in positive column plasmas J. Phys. D: Appl. Phys. 32 2737
- [31] Bogdanov E A *et al* 2004 The influence of metastable atoms and the effect of the nonlocal character of the electron distribution on the characteristics of the positive column in an argon discharge *Tech. Phys.* **49** 698
- [32] Yao J, Yan C, Yuan C, Bogdanov E A, Rabadanov K, Chu Z and Kudryavtsev A 2023 Specificity of the electron energy distribution function in a low-pressure nitrogen plasma Plasma Sources Sci. Technol. 32 055006
- [33] Kolobov V I, Arslanbekov R R, Levko D and Godyak V A 2020 Plasma stratification in radio-frequency discharges in argon gas J. Phys. D: Appl. Phys. 53 25LT01
- [34] Jovanovic A P, Hoder T, Höft H, Loffhagen D and Becker M M 2023 Formation mechanisms of striations in a filamentary dielectric barrier discharge in atmospheric-pressure argon Plasma Sources Sci. Technol. 32 055011
- [35] Golubovskii Y, Kalanov D and Maiorov V 2017 Radial structure of the constricted positive column: modeling and experiment *Phys. Rev.* E 96 023206